International Journal of Gas Turbine, Propulsion and Power Systems
February 2012, Volume 4, Number 1

Effect of Injection Parameters on Jet Array Impingement Heat Transfer

Yoshisaburo Yamane[1], Yoshiyasu Ichikawa[1], Makoto Yamamoto[2] and Shinji Honami[2]

[1] Department of Mechanical Engineering
Graduate School of Engineering, Tokyo University of Science
1-14-6 Kudankita, Chiyoda-ku, Tokyo 102-0073, JAPAN
[2] Tokyo University of Science

ABSTRACT

The purpose of the present study is to clarify the heat transfer characteristics with multiple jet impingement aiming at the highly efficient cooling performance. In the study, we investigated the effect of injection parameters on circular jet array impingement heat transfer. As we focus on interference among the adjacent impinging jets, tests are mainly conducted at the minimum crossflow condition. The experiments are also conducted at injection distance from 2 to 8 jet hole diameters and jet-to-jet spacing from 4 to 8 jet hole diameters. Jet hole diameter Reynolds number is 4,680. Thermochromic liquid crystal is used to obtain heat transfer coefficient. Wall pressure measurement and oil flow visualization on the target surface are performed to understand the flow pattern of impinging jet and wall jet. The effect of injection parameters, such as injection distance, jet-to-jet spacing and number of jets, on jet array impingement heat transfer is clarified.

NOMENCLATURE

A_f	= jet exit area ratio to target surface area, $A_f = \pi D^2/4S^2$
C_p	= wall pressure coefficient, $C_p = 2(P_w - P_{ref})/\rho U_{ref}^2$
D	= jet hole diameter, m (D = 3 mm)
h	= local heat transfer coefficient, W/m^2 K
k	= thermal conductivity of air, W/m K (k = 0.0272 in this study)
L	= injection distance from nozzle to target surface, m
N	= number of jet holes
Nu	= local Nusselt number, Nu = hD/k
$\overline{\mathrm{Nu}}$	= area averaged Nusselt number
$\overline{\mathrm{Nu}}_{4D}$	= 4D-square area averaged Nusselt number (origin of area is center of central jet.)
P_{ref}	= reference pressure (= ambient pressure), Pa
P_w	= local pressure on target surface, Pa
q_w	= heat flux supplied to heat transfer surface, W
Re	= Reynolds number based on jet hole diameter
S	= jet-to-jet spacing, m
T_j	= jet temperature, K
T_w	= target surface wall temperature, K
U_{ref}	= jet velocity, m/s (U_{ref} = 25 m/s)
X	= streamwise distance, normal to target surface, m
Y	= horizontal spanwise distance, along target surface, m
Z	= vertical spanwise distance, along target surface, m
ρ	= density of air, kg/m^3

Presented at International Gas Turbine Congress 2011 Osaka, November 13-18, Osaka, Japan, IGTC2011-0228
Review completed February 15, 2012

INTRODUCTION

In order to improve the performance of the jet engine, it is necessary to increase turbine inlet temperature and to improve the efficiency of its components. Therefore, it is desirable to develop the more efficient cooling mechanism by the minimum mass flow rate of coolant. The impingement cooling system is applied to the inside of turbine blade and combustion liner even now. One of the main reasons is that the impinging jet has the most efficient cooling performance based on the high kinetic momentum. It also has an advantage of a simplified structure. So, an array of the impinging jets has been widely used to provide an effective cooling performance for the hot part of industrial product.

However, the array of impinging jets produces the crossflow due to the existence of the spent flow passing through a confined channel wall and fountain introduced by the impingement of wall jets. It is well known that the presence of the crossflow tends to disturb the impinging jet flow pattern, thicken wall boundary layers and degrade heat transfer rates. And the presence of the fountain also tends to affect the impinging jet behavior, weaken kinetic momentum and cause a distortion of the impinging jet. Since these behaviors cause a degradation of heat transfer on the impingement surface, various remedies are proposed. Uysal et al. [1] made experiment on an in-line array varying the jet hole-size in a systematic manner. They show the influence of the flow rate varied by the jet hole-size on the crossflow. Esposito et al. [2] performed experiment on four types of injection plate with in-line arrays. They show the heat transfer improvement by changing the configuration of the injection plate. Rhee et al. [3] conducted experiment at square arrays with extraction holes on the injection plate. They show that effusion holes play an important role in inhibiting a generation of the crossflow and give a high heat transfer at the narrow injection distance.

The purpose of our study is to investigate the heat transfer characteristics for the highly efficient cooling performance with multiple jet impingement. In the current study, we investigate the effect of injection parameters on the heat transfer of target surface under interference among the adjacent impinging jets. To clear the effect of the interference, we select a minimum crossflow configuration, which is insensitive to the crossflow, for multiple impinging jet arrays. Steady state thermochromic liquid crystal method is employed to obtain heat transfer coefficient. Wall pressure measurement and oil flow visualization on the target surface are conducted to understand the flow pattern of impinging jet and wall jet. We clarify the effect of injection distance, jet-to-jet spacing and number of jets on jet array impingement heat transfer.

EXPERIMENTAL APPARATUS

Test section

Figure 1 shows the test section and coordinate system. The experiments are carried out using a horizontal air blowing nozzle with an injection plate attached to the flow channel exit. The injection plate is exchangeable to conduct the different jet-to-jet spacing experiments. The injection distance is adjusted with the traversing arrangement which the target plate can be moved. The injection plates are formed by 7×7, 5×5 and 3×3 square arrays of circular holes. The jet hole diameter is 3mm. The hole length to diameter ratio is five, and the holes have the chamfered jet inlet edge. The experiments are made at injection distance from 2 to 8 jet hole diameters and jet-to-jet spacing from 4 to 8 jet hole diameters. Spent air was exhausted along the target surface without the interruption such as confined side walls. The velocity at the exit of the hole was 25 m/s, and the Reynolds number based on the jet hole diameter was 4,680. The coordinate origin is located at the center of the central hole exit.

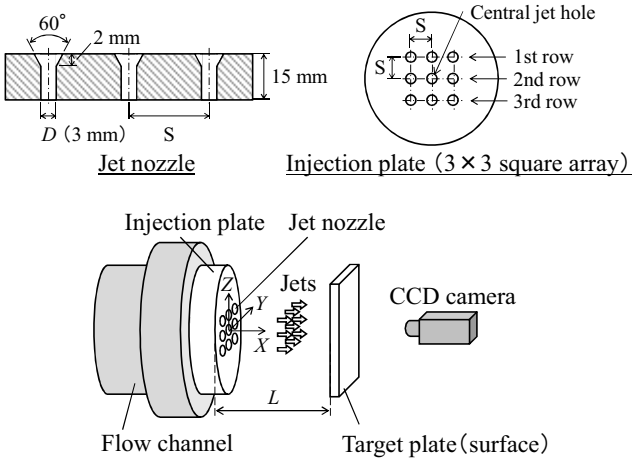

Fig. 1 Test section

Heat transfer measurement

Fig. 2 shows the target surface structure for the heat transfer measurement. The glass is covered with thermochromic liquid crystal sheet and tin dioxide (SnO_2) thin film. The heating area is 120 mm × 130 mm. An air layer between glass and acrylic plate is arranged as thermal insulator. The uniform heat flux is achieved by applying electric current to the electrodes on the SnO_2 thin film. The image of the liquid crystal sheet is recorded by a digital 3CCD color camera in order to measure the temperature distribution of the impingement surface. The image area of each pixel is 0.1 mm × 0.1 mm. Two sets of white LED array are applied for lighting equipment.

The calibration is conducted to convert the color of the liquid crystal to the temperature using the neural network method. Hayashi et al. [4] give clear details about this method. The same method is applied to get the temperature. The 89 images are recorded and measured temperature with a copper-constantan thermocouple (0.2 mm in diameter) attached to the liquid crystal sheet at the same point. The temperature range is from 30.5 °C (303.7 K) to 42.5 °C (315.7 K). The learning frequency is 20,000 times. The standard deviation of the error is 0.043. The color image is converted to the target surface wall temperature by the calibration result. The jet temperature is measured at the upstream of the jet. Nusselt number based on the jet hole diameter is given by Eq. (1).

$$\mathrm{Nu} = \frac{hD}{k} = \frac{q_w}{T_w - T_j} \bullet \frac{D}{k} \tag{1}$$

In this experiment, the estimated total loss of conduction and radiation is less than 4 % of the total imposed net heat flux.

Oil flow visualization

Oil flow technique is used to visualize the surface flow on the target plate. A thin layer of the silicon oil mixed with particles of titanium dioxide is applied to the acrylic target plate. The appearance of the flow is recorded by the same image acquisition system used in the heat transfer measurement. Then, pictures of the path line on the target surface are obtained.

Wall pressure measurement

Wall pressure is measured by a micro differential pressure transducer with a resolution of 0.1 Pa. The target plate is made of acrylic plastic. The target surface has pressure holes of 0.5 mm in diameter at 6 mm intervals. Pressure distribution is obtained at 1 mm intervals with the traversing arrangement. Wall pressure coefficient is given by Eq. (2).

$$C_p = \frac{2(P_w - P_{ref})}{\rho U_{ref}^2} \tag{2}$$

Measurement uncertainties

An estimate of the uncertainties associated with the experiments has been made using the method of small perturbations described by Moffat [5]. Calculations were performed to estimate the uncertainties in typical experimental parameters at the test conditions using the similar approach taken by Chambers et al. [6]. The typical RSS (Root Sum Square) error in the Nu number measurements is 13.51 %, and in the worst case this rises 21.41 %. The results of the uncertainty analysis are presented in Table 1.

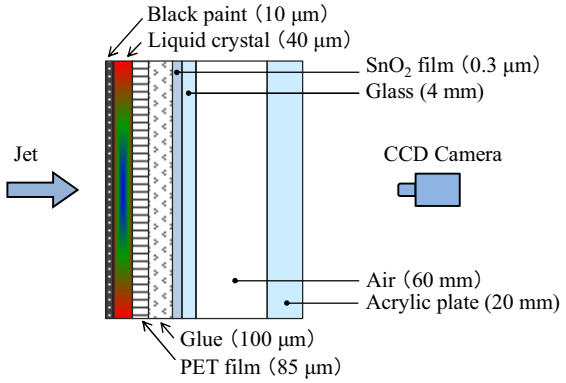

Fig. 2 Target surface structure for heat transfer measurement

Table. 1 Uncertainty analysis for Nusselt number measurements

Parameters	Typical value	Typical error	Error in Nu [%]
q_w [W/m^2]	1049.7	0.12	0.01
T_w [K]	311.2	0.54	8.20
T_j [K]	305.1	0.53	10.41
D [m]	0.003	0.50×10^{-5}	0.15
k [W/m^{2}K]	0.0272	0.74×10^{-3}	2.64
		RSS error	13.51
		Max error	21.41

RESULT AND DISCUSSIONS

Local heat transfer coefficient

Figs. 3 (a)-(c) show the local Nusselt number contours on the target surface at L/D = 2. Figs. 4 (a)-(c) show the spanwise

distributions of the local Nusselt number for different jet-to-jet spacing at L/D = 2. These are 3×3 square arrays (N = 9) cases. On the whole, high Nusselt number is observed at the impingement point and gradually decreases as the position moves apart from the impingement stagnation point. Fig. 3 (a) shows that relatively high Nusselt number (around Nu = 25) is widely spread on the target surface. Fig. 4 (a) shows that the gap between maximum and minimum Nusselt number becomes narrow in the case of jet-to-jet spacing S/D = 4 compared with the cases of S/D = 6 to 8 (Figs.4 (b)-(c)). However at wide jet-to-jet spacing S/D = 8, local Nusselt number is maximal at the stagnation point (Fig. 3 (c) and Fig. 4 (c)). These tendencies are similar to the cases at the long injection distance L/D = 4 to 8, as shown in Figs. 5 (a)-(c) and Figs. 6 (a)-(c). These phenomena are due to interference of the adjacent impinging jets.

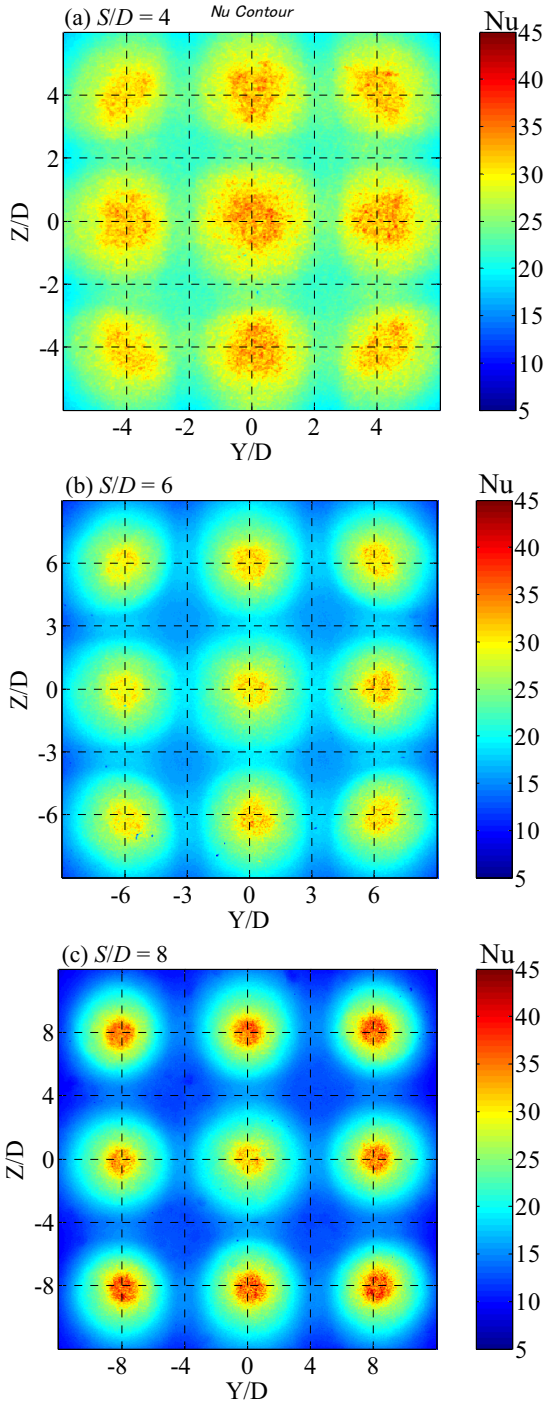

Fig. 3 Local Nusselt number contour on target surface at L/D = 2

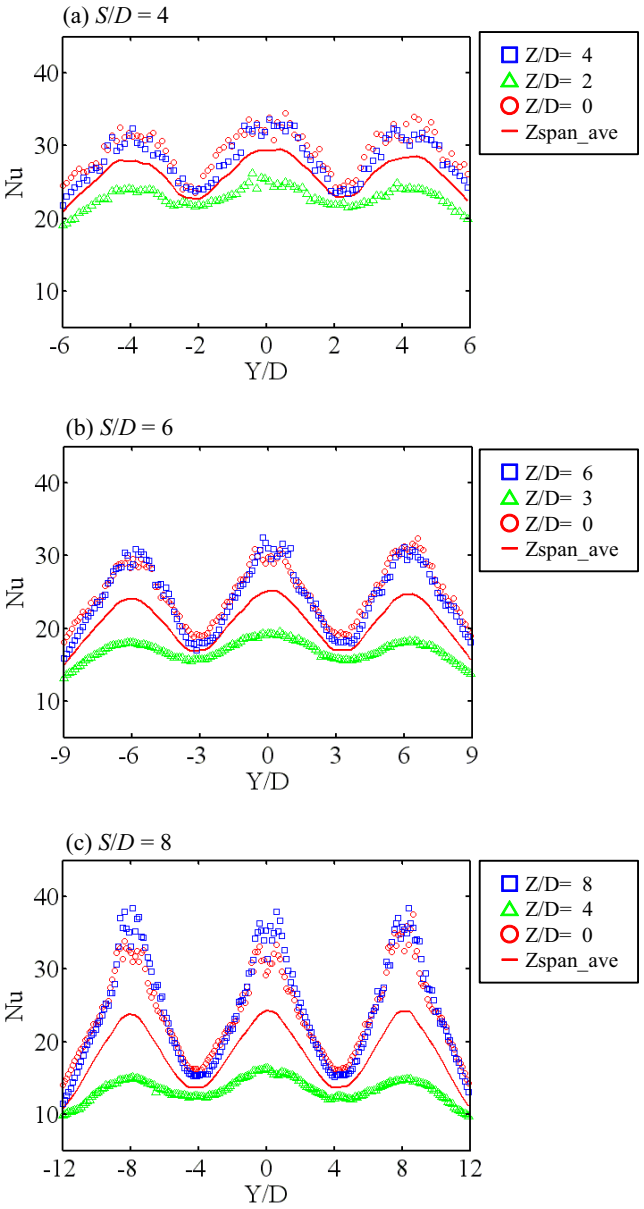

Fig. 4 Spanwise distributions of local Nusselt number in a one- row configuration for different injection distances at L/D =2 (circle: second row, triangle: mid line between first and second row, square: first row, line: spanwise Z direction average from first row to third row)

Average heat transfer coefficient

Fig. 7 shows the area averaged Nusselt number based on the ratio of jet exit area to target surface area A_f. Eight cases of the square arrays pattern were compared with literature datum from Kercher et al. [7], Martin et al. [8] and Obot et al. [9]. Fig. 7 shows the comparison of the present data and published results. Every case corresponds to the condition of minimum cross flow. The difference of the area averaged Nusselt number between the cases S/D = 6 (N = 9) and S/D = 6 (N = 25) caused by the number of jets which affects the mass flow of total cooling air. So, the present results agree well with literature datum.

Fig. 8 indicates that area averaged Nusselt number becomes low with the increase of jet injection distance from nozzle to target surface. In the cases of S/D = 6 to 8, area averaged Nusselt number reaches a ceiling at around L/D = 4. In the case of S/D = 4, however, area averaged Nusselt number suddenly increases at L/D = 2. This phenomenon appears to be the distinctive characteristics by

interference of the adjacent impinging jets.

Fig. 9 presents another area averaged Nusselt number to support the characteristics described above. We define the average area as 4*D*-squared. The origin of the area is the center of the central jet. The 4*D*-square area averaged Nusselt number gives the effect of central jet on the impinging heat transfer. Fig. 9 shows a similar trend to that in Fig. 8, but regardless of the different jet-to-jet spacing, the 4*D*-square area averaged Nusselt numbers are almost equal in the case of $L/D = 8$. This implies there is little effect on the central jet by the surrounding jets.

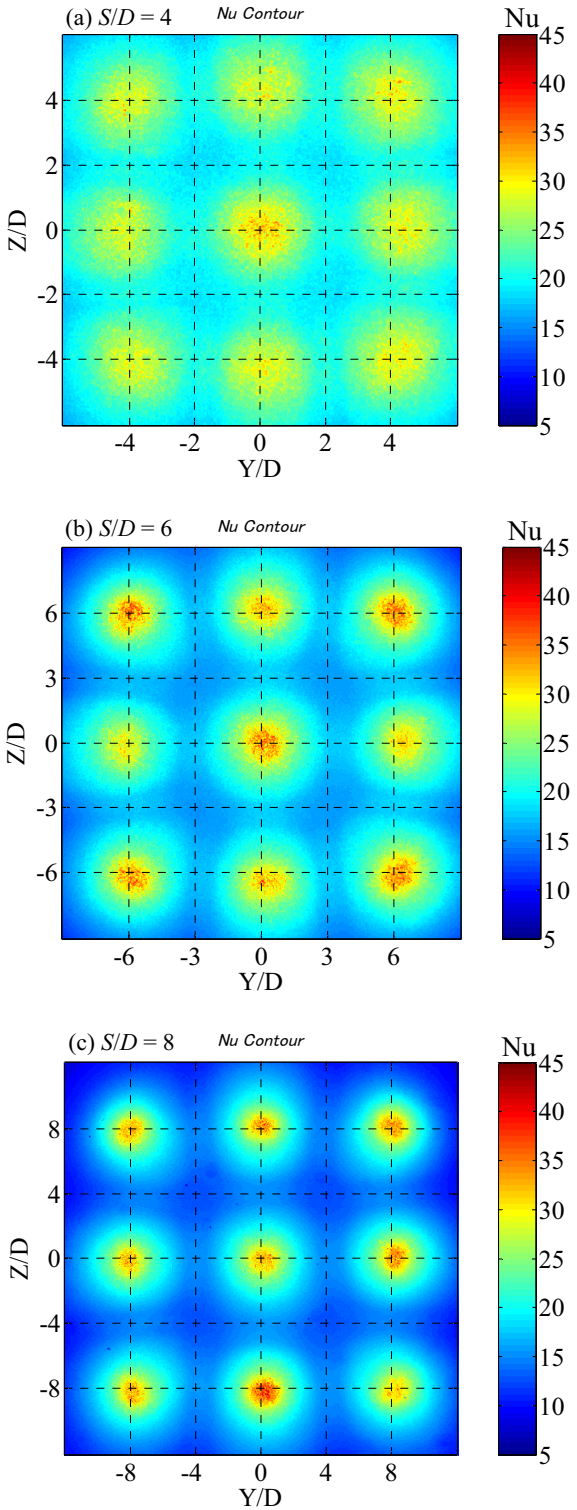

Fig. 5 Local Nusselt number contour on target surface at $L/D = 6$

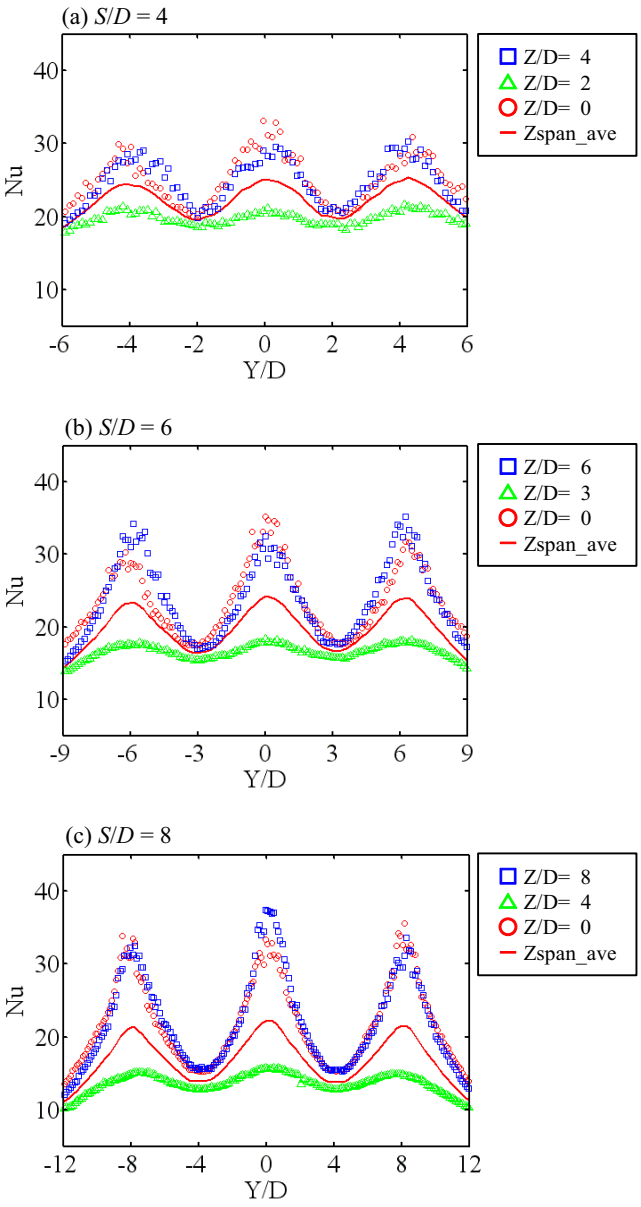

Fig. 6 Spanwise distributions of local Nusselt number in a one- row configuration for different injection distances at $L/D = 6$ (circle: second row, triangle: mid line between first and second row, square: first row, line: spanwise Z direction average from first row to third row)

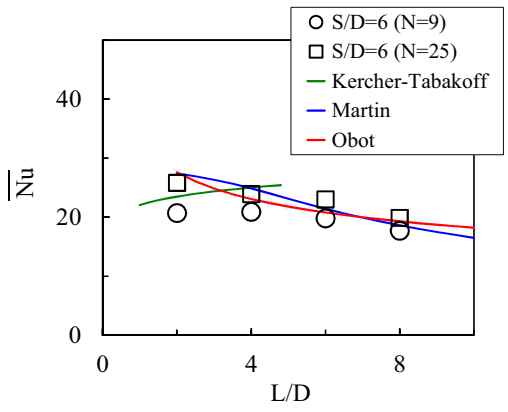

Fig. 7 Area averaged Nusselt number for $A_f = 0.022$ and Re = 4,680

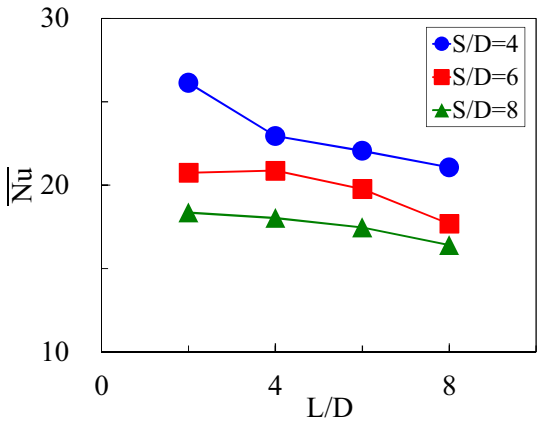

Fig. 8 Area averaged Nusselt number

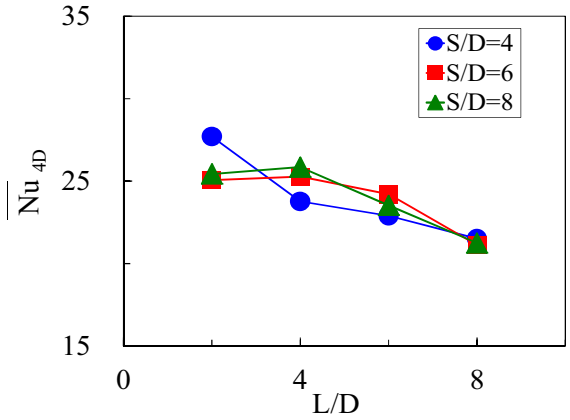

Fig. 9 4D-square area averaged Nusselt number

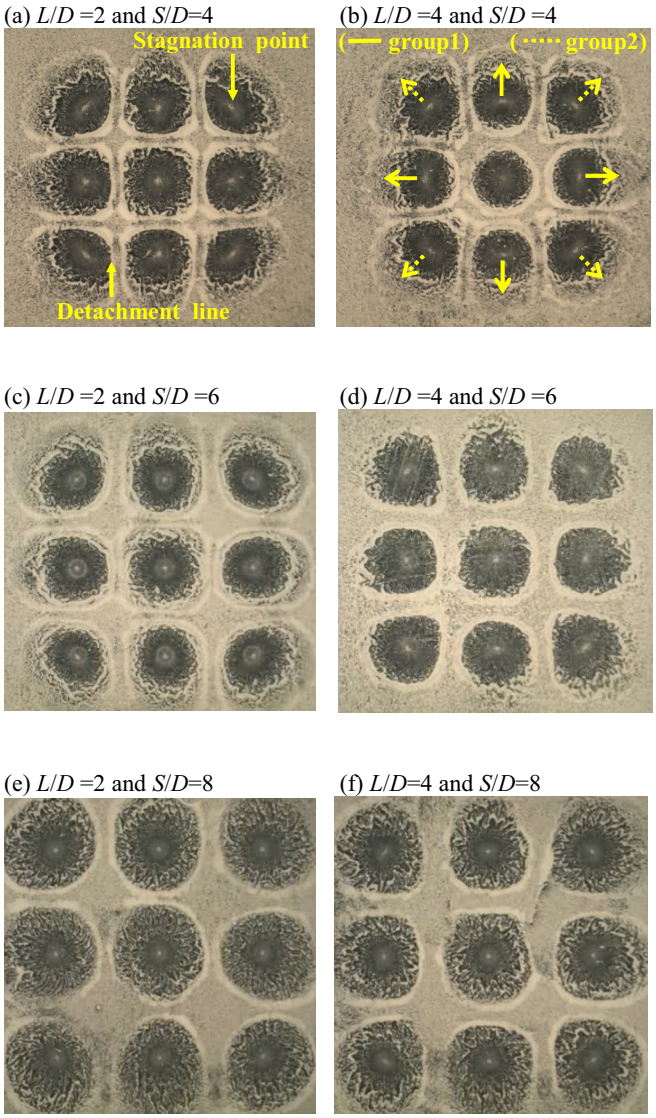

Fig. 10 Path line of impinging jets and wall jets by oil flow pictures

Oil flow visualization

Oil flow visualization was conducted on the target surface to investigate the flow behavior due to interference among the adjacent impinging jets. Figs. 10 (a)-(f) show the path lines of the impinging jets and wall jets for L/D = 2 and 4. These pictures indicate the stagnation point of impinging jet and the detachment line caused by the impingement of adjacent wall jets.

Geers et al. [10] obtained mean flow field and the distribution of turbulence kinetic energy in vertical planes to the target surface with particle image velocimetry (PIV) at similar configuration (L/D = 4, S/D = 4, Re = 20,000 and 3×3 square arrays of circular orifice). They indicated a clear distortion of the outer jets caused by the impingement of the wall jets. The impingement introduces an upwash motion which is called as "fountain" (cf. Fig. 11) here after and recirculation in the region between the jets. We compared the "shift" (cf. Fig. 11) of the stagnation point with geometrically-based injection jet hole position to confirm the influence of the distortion on the target surface heat transfer. Fig. 12 shows the results (the direction of shift is shown by arrows in Fig. 10 (b)).

There exist two types of jet at the outer periphery arrays. One is surrounded by five jets and the other is surrounded by three jets. So, we defined the former as group 1 and the latter as group 2. The shift of group 1 gradually increase except for S/D = 4. This means that wall jet interference is observed in the group 1 jets, because the

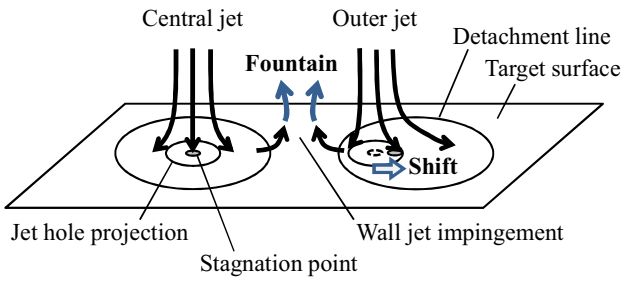

Fig. 11 Schematics of "fountain" and "shift"

clearance from the central jet is narrower than that of group 2. In the case of L/D = 2 in the group 1, however, all the displacements approach zero. It is presumed that the strength of jet velocity (kinetic momentum) defeats the effect of the fountain due to the short injection distance.

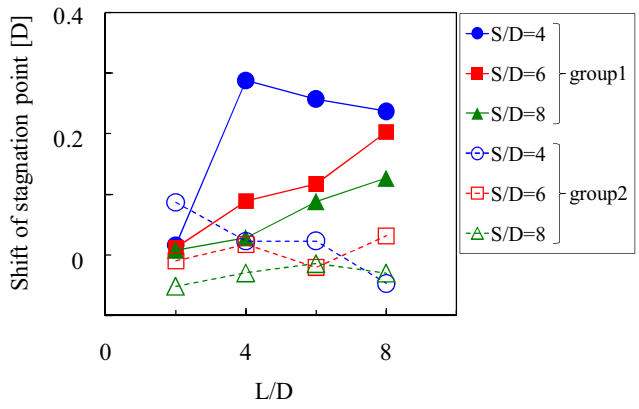

Fig. 12 Comparison of shift of stagnation point with geometrically-based injection jet hole position

Wall pressure coefficient

The wall pressure coefficient was measured to investigate the effect of the fountain caused by the impingement of the adjacent wall jets. Figs.13 (a)-(d) show comparison of wall pressure coefficient distribution on the target surface for different jet-to-jet spacing at $Z/D = 0$. The measurement is conducted only at the first quadrant area and only at the spanwise Y direction because of its symmetry distribution which is confirmed by oil flow visualization. Fig. 13 (a) shows that wall pressure coefficient between the jets has a bump as shown by an arrow at the jet-to-jet spacing $S/D = 4$. There, maximum C_p is 0.1. The bump's height is decreased as the S/D becomes wider. This implies that the strength of the wall jets interference becomes weak. Fig.13 (d) shows the wall pressure coefficient of the single impinging jet. This distribution indicates that the impinging jet velocity (kinetic momentum) is maintained without loss showing C_p of almost 1.0 at the stagnation point for $L/D = 2$ to 8 if there is no surrounding jet. Therefore, the shift of the stagnation point indicates the strength of the wall jet interference, and wall pressure coefficient is reduced significantly with the increase of the injection distanse for the narrow jet-to-jet spacing at the stagnation point.

Wall jets interference between adjacent impinging jets

Fig. 14 shows local Nusselt number at the stagnation point of the central jet. In general, the stagnation point Nusselt number for the single impinging jet gives the maximum value in the injection distance $L/D = 4$ to 8. All the jet-to-jet spacing cases show that their maximum peaks exist in their forementioned range except for the case of $S/D = 4$. This indicates that the promotion of the heat transfer at $L/D = 2$ and $S/D = 4$ occurs due to interference between the adjacent jets. According to the results of San et al. [11], the Nusselt number at the stagnation point of the central jet indicates the maximum in the case of $S/D = 8$. They employed injection parameters with $L/D = 2$, $S/D = 4$ to 16, Re = 10,000 and staggered arrays of five circular orifices. In the present case of $L/D = 2$ at $S/D = 4$, as the number of adjacent surrounding jets is larger than that of San's experiment, interference between the adjacent jets introduces an increase of the Nusselt number at the stagnation point.

At the location of the wall jets impingement, Bernard et al. [10] shows the schema of the flow near an impingement zone with Laser-Doppler Anemometer and laser sheet visualizations. Their experimental condition corresponds to a maximum cross flow with the range of $L/D = 2$, $S/D = 4$, Re = 12,600 and 3×5 square arrays of circular orifice. They indicate the rolling-up (upwash) fountain caused by the impingement of the wall jets and the vortex pairs beneath the fountain. The upwash fountain leads to the recirculation in the region next to the impinging jet. The vortex pairs lead to downwash. Figs. 13 (a)-(c) show the existence of downwash motion typically in the case of $S/D = 4$ and slightly in

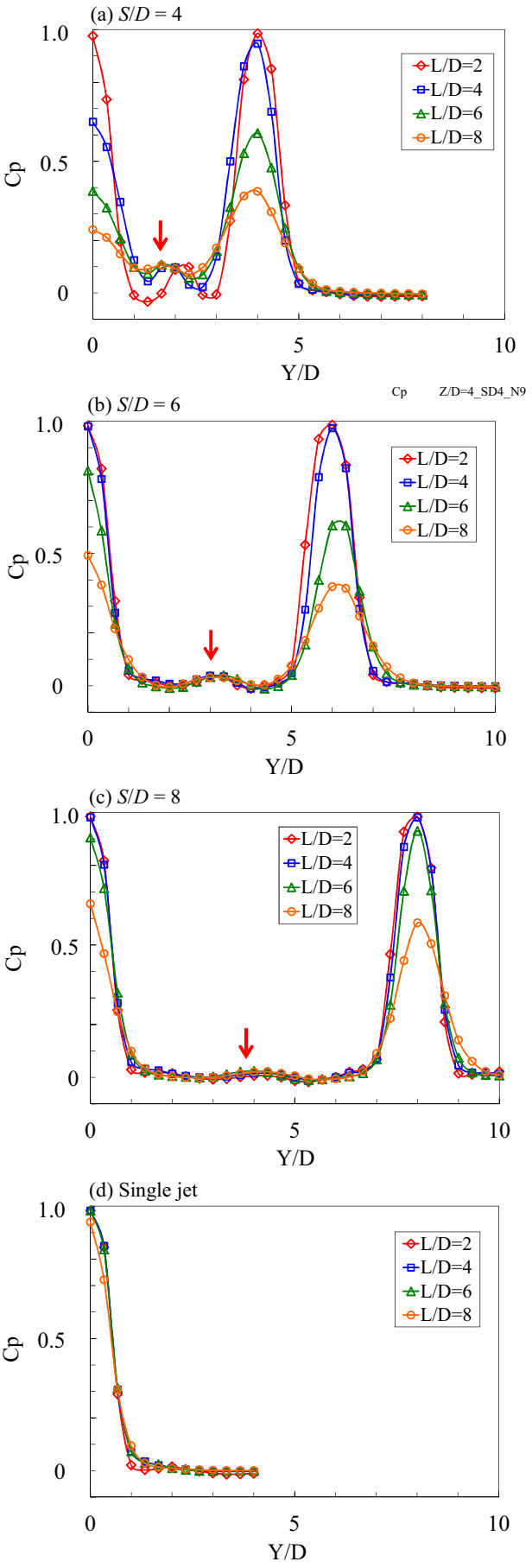

Fig. 13 Comparison of wall pressure coefficient C_p distribution on target surface ($Z/D = 0$)

the cases of S/D = 6 and 8. This phenomenon makes the gap between maximum and minimum of the local Nusselt number narrow in the case of jet-to-jet spacing S/D = 4 compared with in the cases of S/D = 6 and 8 at constant injection distance as shown in Figs. 4 (a)-(c) and Figs. 6 (a)-(c).

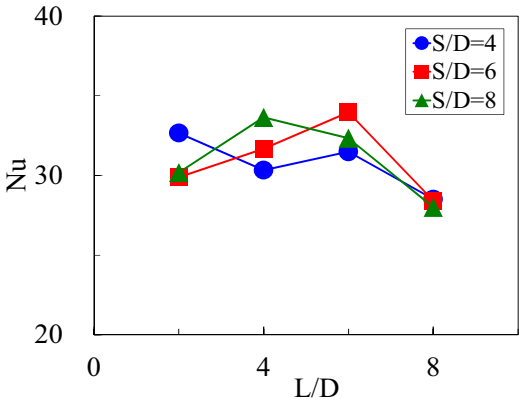

Fig. 14 Local Nusselt number at stagnation point of central jet

The effect of the surrounding jets array number

The more number of arrays of jets increases, the more strength of wall jets interference increases. Here, we investigate the effect of the number of arrays on the impinging heat transfer coefficient. Fig. 15 shows area averaged Nusselt numbers of different surrounding areas in the cases of 7×7 square arrays (S/D = 4) and 5×5 square arrays (S/D = 6) at constant A_f, respectively. There is no change in the area averaged Nusselt number among the cases at this minimum cross flow condition.

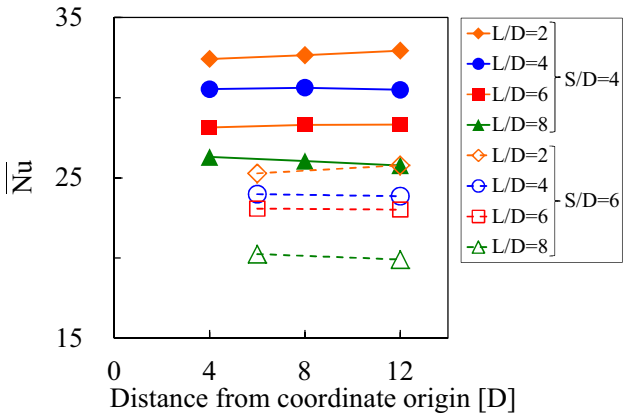

Fig. 15 Comparison of area averaged Nusselt number for different distance from coordinate origin at constant A_f each for 7×7 square arrays (S/D = 4) and 5×5 square arrays (S/D = 6)

Figs. 16 (a)-(c) show the local Nusselt number contours on the target surface. Figs. 17 (a)-(c) show the spanwise distributions of local Nusselt number for different injection distances at S/D = 4. The tendency of the local Nusselt number distribution is quite similar to that of 3×3 square arrays. It is also found that the local Nusselt number becomes higher at the impingement point and gradually decreases as the position moves apart from the stagnation point. And Figs. 17 (a)-(c) show that the local Nusselt number at the stagnation point decreases as the injection distance becomes longer. Moreover, the local Nusselt number gets higher at the outer periphery arrays and the highest at the outer corner jets.

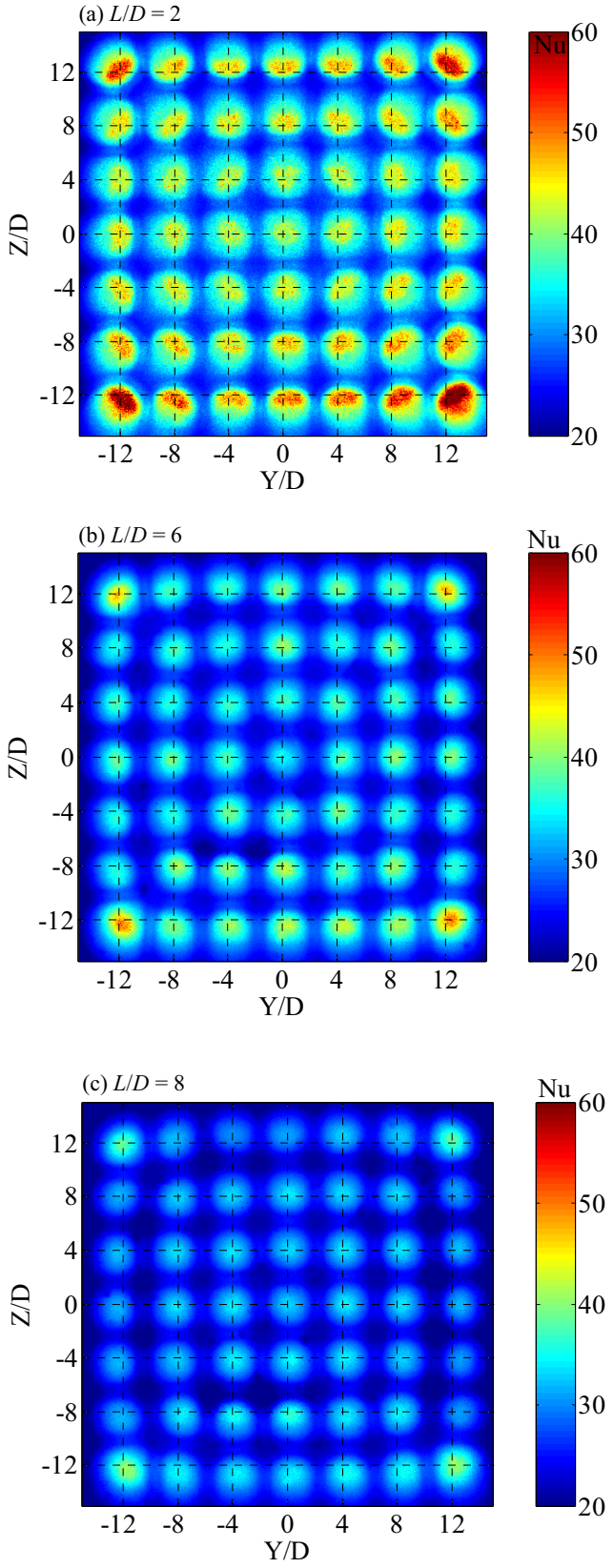

Fig. 16 Local Nusselt number contour (S/D = 4 and N = 49) on target surface

This phenomenon is caused by the small number of the adjacent surrounding jets and absence of the confined side walls. Therefore, the outer periphery arrays of the jets and the outer corner jets are allowed to behave somewhat like a single jet. This tendency is different from the case in the maximum cross flow.

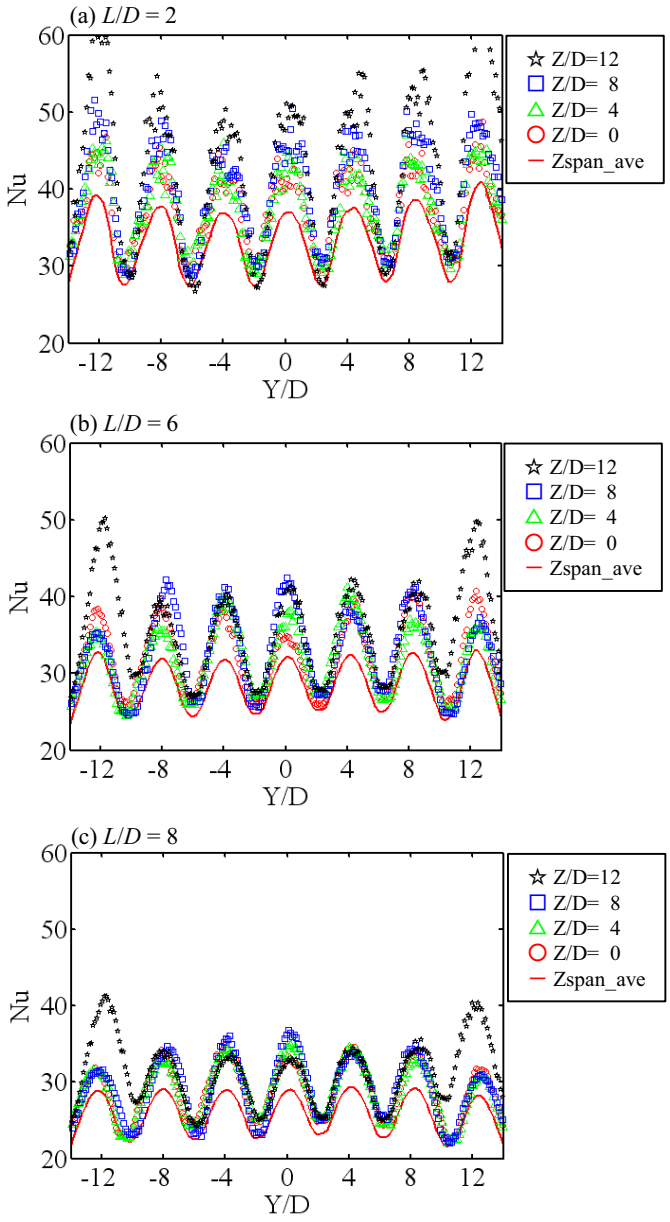

Fig. 17 Local Nusselt number contour (S/D = 4 and N = 49) on target surface (circle: fourth row, triangle: third row, square: second row, star: first row, line: spanwise Z direction average from first row to seventh row)

CONCLUSIONS

This paper discussed the effect of injection parameters on jet array impingement heat transfer. In the case of square arrays of circular impinging jets, the strength of jet velocity (kinetic momentum) normal to the target surface and the fountain introduced by the impingement of wall jets strongly affect the heat transfer on the target surface. When the injection distance is short, the position of the jet stagnation point does not shift. The jet velocity is maintained its strength and is little affected by the fountain. On the other hand, when the jet-to-jet spacing is short, the effect of fountain becomes stronger. The following conclusions are obtained in this study.

(1) 3×3 square arrays (N = 9) case

- The gap between maximum and minimum Nusselt number becomes narrow and area averaged Nusselt number is high in the case of jet-to-jet spacing S/D = 4 compared with the cases of S/D = 6 and 8.
- Wall jets interference shows a strong effect in the case of S/D = 4, but little effect in the cases of S/D = 6 and 8.
- In the case of S/D = 4, the area averaged heat transfer coefficient at L/D = 2 shows a distinguished increase compared to any other jet-to-jet spacing owing to the vortex pairs beneath the upwash fountain.
- In the case of short injection distance L/D = 2, the stagnation point of the impinging jet stays and keeps its nominal geometric jet-to-jet spacing in the cases of S/D = 4 to 8.

(2) 5×5 and 7×7 square arrays (N = 25 and 49) cases

- The area averaged Nusselt number is varied only slightly as the average area is increased.
- The local Nusselt number is higher at the outer periphery arrays and the highest at the outer corner jets.

REFERENCES

[1] Uysal, U., Li, P. W., Chyu, M. K., Cunha, F. J., 2006, "Heat Transfer on Internal Surfaces of a Duct Subjected to Impingement of a Jet Array with Varying Jet Hole-Size and Spacing," *ASME Journal of Turbomachinery*, Vol. 128, pp. 158-165.

[2] Esposito, E. I., Ekkad, S. V., Kim, Y., Dutta, Partha, 2009, "Novel Jet Impingement Cooling Geometry for Combustor Liner Backside Cooling," *ASME Journal of Thermal Science and Engineering Applications*, Vol. 1, pp. 021001-1-8.

[3] Rhee, D. H., Yoon, P. H., Cho, H. H., 2003,"Local Heat/Mass Transfer and Flow Characteristics of Array Impining Jets with Effusion holes Ejecting Spent Air," *International Journal of Heat and Mass Transfer*, Vol. 46, pp. 1049-1061.

[4] Hayashi, T., Taki, J., Motosuke, M., Honami, S., 2009, "Experimental Study on Control of an Impinging Jet Heat Transfer Using Triangular Tabs," *JSME Journal of Fluid Science and Technology*, Vol. 4, pp. 292-303.

[5] Moffat, R. J., 1988, "Describing the Uncertainties in Experimental Results," *Experimental Thermal and Fluid Science*, Vol. 1, pp.3-17.

[6] Chambers, A. C., Gillespie D. R. H., Ireland P. T., Dailey G. M., 2005, "The Effect of Initial Cross Flow on the Cooling Performance of a Narrow Impingement Channel," *ASME Journal of Heat Transfer*, Vol. 127, pp. 358-365.

[7] Kercher, D. M., Tabakoff, W., 1970, "Heat Transfer by a Square Array of Round Air Jets Impinging Perpendicular to a Flat Surface Including the Effect of Spent Air," *ASME Journal of Engineering for Power*, Vol. 92, pp. 73-82.

[8] Martin, H., 1977, "Heat and Mass Transfer Between Impinging Gas Jets and Solid Surfaces," *Advances in Heat Transfer*, Vol. 13, pp 1-60.

[9] Obot, N. T., Trabold, T. A., 1987, "Impingement Heat Transfer Within Arrays of Circular Jets: Part 1 - Effects of Minimum, Intermediate, and Complete Crossflow for Small and Large Spacings," *ASME Journal of Heat Transfer*, Vol. 109, pp. 872-879.

[10] Geers, L.F.G., Hanjalic, K., Tummers, M. J., 2005, "Wall Imprint of Turbulent Structures and Heat Transfer in Multiple Impinging Jet Arrays," *Journal of Fluid Mechanics*, Vol. 546, pp. 255-284.

[11] San, J. Y., Lai, M. D., 2001, "Optimum Jet-to-jet Spacing of Heat Transfer for Staggered Arrays of Impinging Air Jets," *International Journal of Heat and Mass Transfer*, Vol. 44, pp 3997-4007.

[12] Bernard, A., Brizzi, L. E., Bousgarbies, J. L., 1999, "Study of Several Jets Impinging on a Plane Wall: Visualizations and Laser Velocimetry Investigations," *ASME Journal of Fluids Engineering*, Vol. 121, pp. 808-812.